



1 **Glacier surges on James Ross Island, Antarctica, and their** 2 **relationship with climate**

3 Benjamin J. Davison¹, Andrew J. Sole¹, Gregoire Guillet², Douglas I. Benn³, Jonathan
4 Kingslake^{4,5}, Jeremy C. Ely¹, Stephen J. Livingstone¹, Christopher D. Stringer⁶, Jonathan L.
5 Carrivick⁷, Anna E. Hogg⁸

6 ¹School of Geography and Planning, University of Sheffield, Sheffield, UK

7 ²Department of Geosciences, University of Oslo, Oslo, Norway

8 ³School of Geography and Sustainable Development, University of St Andrews, St Andrews, UK

9 ⁴Lamont-Doherty Earth Observatory, Columbia University, New York, USA.

10 ⁵Department of Earth and Environmental Science, Columbia University, New York, USA

11 ⁶School of Built Environment, Engineering and Computing, Leeds Beckett University, Leeds, UK

12 ⁷School of Geography and water@leeds, University of Leeds, Leeds, UK

13 ⁸School of Earth, Environment and Sustainability, University of Leeds, Leeds, UK

14 *Correspondence to:* Benjamin J. Davison (b.j.davison@sheffield.ac.uk)

15 **Abstract.** Although the Antarctic Peninsula has a similar climate to that of other regions hosting surge-
16 type glaciers, only one glacier surge has been previously observed in this region. We examined ice
17 surface velocity, elevation and terminus position changes of Antarctic Peninsula glaciers to identify
18 glacier surges. This revealed only four surges from three glaciers, all on James Ross Island. Gourdon
19 Glacier surged from 2005 to 2007 then again from 2013 to 2018, Kotick Glacier surged during 2013 to
20 2017 and Whisky Glacier surged from 2020 to 2024. All four surges were characterised by significant
21 advances in glacier terminus position and, for the latter three surges where observations are more
22 abundant, at least an order-of-magnitude speed-up and mass transfer from upper to lower parts of each
23 glacier. The landform record and historical imagery suggest additional surges of Kotick Glacier and
24 Gourdon Glacier may have occurred in the second half of the 20th century. Reanalyses, reconstructions
25 and observations of air temperature suggest that atmospheric warming since 1940 has increasingly
26 exposed these and neighbouring glaciers on the northern tip of the Antarctic Peninsula and its
27 surrounding islands to conditions that are typical of surge-type glaciers globally. Climate projections
28 indicate that future warming will expose more glaciers on the Peninsula to climatic conditions
29 conducive to surging until the mid-20th century, after which the surge-conducive area remains steady
30 under Shared Socioeconomic Pathway (SSP) 2-4.5 and declines under SSP5-8.5. This suggests that
31 surges on the Antarctic Peninsula may become more common over the coming decades, motivating
32 continued monitoring.

33 **1 Introduction**

34 Glaciers on the Antarctic Peninsula have undergone large changes in ice motion and geometry on
35 seasonal to decadal timescales that are driven by a range of atmospheric and oceanic processes. Notable



36 glacier dynamic changes have included the retreat, disintegration and loss of ice shelves principally due
37 to rising air temperature (Cook and Vaughan, Rott et al., 1996; Doake and Vaughan, 1991, Cooper,
38 1997, MacAyeal et al., 2003; Rack and Rott, 2004, Braun et al., 2009) and the consequent short-lived
39 (approximately one year) acceleration, thinning then long-term (decadal) deceleration of their tributary
40 glaciers (Rignot et al., 2004; Scambos et al., 2004; Wuite et al., 2015; Rott et al., 2018; Seehaus et al.,
41 2018). Following their response to the disintegration of the Larsen-B Ice Shelf in 2002, several glaciers
42 in the Larsen-B Embayment underwent a second phase of acceleration in 2022. This renewed speed-up
43 was linked to the evacuation of 11-year-old landfast sea ice, which occurred during a period of
44 anomalously high air temperatures and strong offshore winds (Ochwat et al., 2024; Surawy-Stepney et
45 al., 2024; Sun et al., 2023). On the east coast of the Antarctic Peninsula, atmospheric rivers can drive
46 extreme melt events (Gorodetskaya et al., 2023) even during (austral) winter (Kuipers Munneke et al.,
47 2018). Surface meltwater access to the ice bed may cause short-lived (i.e. lasting less than two weeks)
48 grounded ice acceleration (Tuckett et al., 2019), although this is debated and surface-to-bed meltwater
49 connections through grounded ice have yet to be demonstrated (Rott et al., 2020; Tuckett et al., 2020).
50 Some glaciers, particularly those along the west coast, undergo notable speed-ups during the (austral)
51 summer (Wallis et al., 2023a; Boxall et al., 2022), which in many cases closely follow changes in glacier
52 terminus position, although the drivers remain debated (Boxall et al., 2024). Many glaciers along the
53 west coast have undergone substantial retreat since at least the 1980s (Cook et al., 2005; Cook and
54 Vaughan, 2010; Cook et al., 2016) and exhibited widespread acceleration due to warm water incursions
55 (Hogg et al., 2017) particularly since 2020 (Wallis et al., 2023b; Davison et al., 2024). Thus, Antarctic
56 Peninsula glaciers display a wide range of dynamic behaviours due to their summertime exposure to
57 positive air temperatures, contrasting oceanic settings on the east coast compared to the west coast,
58 significant changes to ice shelf extent and associated buttressing, and variable sea ice conditions.

59 Surge-type glaciers are characterised by phases of rapid ice flow and advance that are separated by
60 much longer periods of quiescence, during which ice flow is typically an order of magnitude slower
61 than the surge phase (Jiskoot, 2011; Guillet et al., 2025). Many theories seeking to explain the timing
62 and mechanism for glacier surging have been proposed (Kamb et al., 1985; Fowler et al., 2001; Murray
63 et al., 2003; Dunse et al., 2015). The enthalpy balance theory for glacier surging proposes that all surge
64 cycles reflect imbalances between the rates that heat and water (enthalpy) are produced at, and are
65 evacuated from, glacier beds (Benn et al., 2019a, 2022). This model is consistent with clustering of
66 surge behaviour in regions with climatic conditions intermediate between cold/dry and warm/humid
67 end members; under intermediate climatic conditions, frictional heating from ice flow can increase
68 enthalpy too fast to be balanced by slow processes such as heat conduction through cold ice, but too
69 slow to sustain fast processes, such as meltwater evacuation through efficient subglacial conduits
70 (Sevestre and Benn, 2015; Guillet et al., 2025). As a result, glaciers oscillate between fast and slow
71 modes of ice flow in order to achieve steady-state mass balance over multi-annual timescales. In the



72 enthalpy balance model of surging, glacier geometry and physical setting play a secondary but important
73 role in dictating the distribution of surge-type glaciers, meaning that climate conditions alone are not
74 expected to be prognostic of surge occurrence – many glaciers exposed to conditions typical of surge-
75 type glacier settings do not surge, presumably because their geometry or underlying geology permit
76 steady-state mass and enthalpy fluxes (Benn et al., 2019a, 2022).

77 Based on glacial geomorphology, Carrivick et al. (2012) questioned why no surge-type behaviour
78 seemed to occur on James Ross Island (JRI), off the north-east coast of the Antarctic Peninsula, and
79 Sevestre and Benn (2015) postulated that glacier surging could occur on the Antarctic Peninsula given
80 that the post-2000 climatic conditions were similar to those observed at other surge-type glaciers
81 globally. Recognition that parts of the Antarctic Peninsula experience a climate typical of surge-type
82 glaciers was reiterated in a more recent review (Lovell et al., 2026). One surge of Kotick Glacier on JRI
83 has been identified based on an observed tripling of ice velocity in 2015 along with frontal thickening
84 and advance (Stringer et al., 2025).

85 Here, we present satellite observations of three glaciers on JRI that show each glacier has surged at least
86 once since 2000. We visually interpret the geomorphological record and glacier terminus position
87 change visible in satellite and aerial imagery to provide evidence of surging in the 20th century and
88 discuss the behaviour of these glaciers in the context of the globally-defined optimal climatic envelope
89 for surge-type glaciers (Sevestre and Benn, 2015; Guillet et al., 2025).

90 **2 Methods**

91 We used existing (Cook et al., 2005; Gardner et al., 2025) and new measurements of ice surface velocity,
92 elevation change and terminus position across the Antarctic Peninsula from 1985 to 2025 to identify
93 potential glacier surges. These data allowed us to identify and characterise surges from three glaciers -
94 Kotick Glacier, Gourdon Glacier and Whisky Glacier - on JRI (Figure 1). The quality and
95 comprehensiveness of the observations generally improved over time as more satellite images became
96 available, which could have resulted in missed surging behaviour prior to, or early in, the observational
97 record. To identify potential 20th century surging behaviour, we supplemented our measurements with
98 visual interpretation of glacial geomorphology, ice margin position and ice surface characteristics using
99 space- and airborne imagery. Finally, we placed the observations of surging behaviour in the context of
100 climatic changes over JRI and the wider region from 1940 to 2150 using ERA5 reanalyses and CMIP6
101 projections under moderate (Shared Socioeconomic Pathway (SSP) 2-4.5) and extreme (SSP5-8.5)
102 warming scenarios.

103 **2.1 Ice velocity**

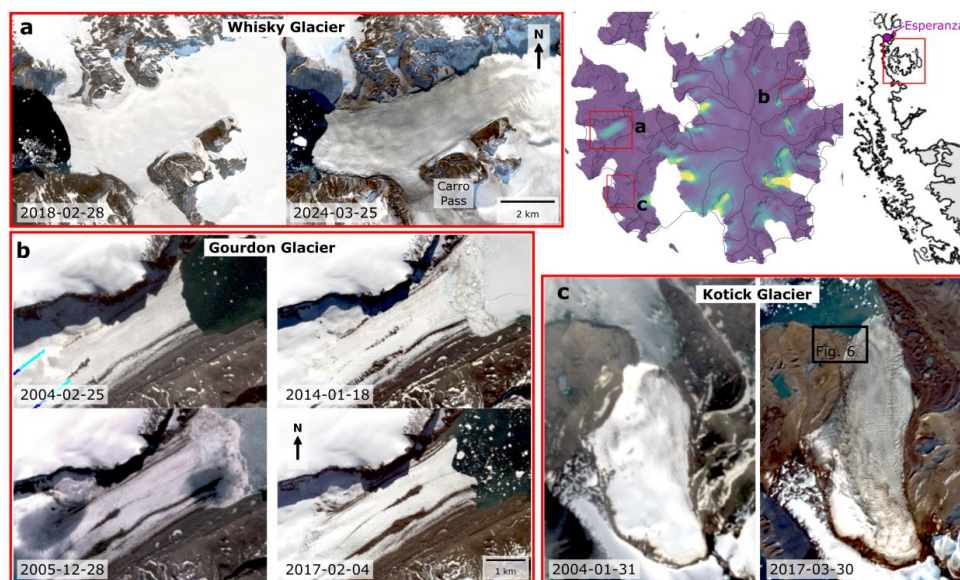


Figure 1. Study area and overview of terminus position change at (a) Whisky Glacier, (b) Gourdon Glacier, and (c) Kotick Glacier (b). The satellite images in (a), (b) and (c) labelled 2018-02-28, 2024-03-25 and 2017-03-30 are true-colour Sentinel-2 images; those labelled 2014-01-18 and 2017-02-04 are true-colour Landsat 8 images; the remainder are true-colour pan-sharpened Landsat 7 images. The upper right panel shows the 2014 to 2025 average ice surface speed on James Ross Island, overlaid on a 10 m Reference Elevation Model of Antarctica hillshade (Howat et al., 2022a), with the locations of panels (a-c) marked and glacier basins (Cook et al., 2014) delineated in black. The inset map shows the outline of the Antarctic Peninsula (Gerrish et al., 2024) with ice shelves (Mouginot et al., 2017) shaded grey and Esperanza Station labelled in magenta.

104 Ice velocity was estimated from feature and speckle tracking of Landsat 8 and 9 (January 2013 to
 105 present) and Sentinel-2 (January 2016 to present) optical image pairs, and Sentinel-1a (April 2014 to
 106 present), Sentinel-1b (October 2016 to December 2021) and Sentinel-1c (December 2024 to present)
 107 Interferometric Wide swath mode Single-Look Complex Synthetic Aperture Radar (SAR) amplitude
 108 image pairs. We supplement our feature tracking with velocity estimates generated as part of the
 109 ITS_LIVE project (Gardner et al., 2025). Prior to tracking, the SAR images were focused and co-located
 110 using the Generic Mapping Toolbox for SAR imagery (GMTSAR; Sandwell et al., 2011a, 2011b) and
 111 the optical images were co-registered by cross-correlating the images over bedrock areas.

112 We oversampled the SAR images in the azimuth direction by a factor of four and used image patch
 113 sizes of 128×512 single-look oversampled azimuth and range pixels, with a step size of 32 and 64
 114 pixels respectively between patches (Davison et al., 2023). For the optical image pairs, we used an
 115 iterative cross-correlation approach with two passes, shifting and deforming the image using
 116 information in the first pass before performing the second pass. We varied the image patch size
 117 depending on the satellite image resolution. For Landsat image pairs, we used image patch sizes of 64
 118 x 64 pixels with a step of 16 pixels in the first pass, then a patch size of 42 x 42 pixels and a step of 6
 119 pixels in the second pass. For Sentinel-2 image pairs, we used image patch sizes of 96 x 96 pixels with



120 a step of 24 pixels in the first pass, then a patch size of 56 x 56 pixels and a step of 8 pixels in the second
121 pass. Tracking of each image patch was undertaken in MATLAB, within a version of PIVsuite
122 (Thielicke & Stamhuis, 2014; <https://uk.mathworks.com/matlabcentral/fileexchange/45028-pivsuite>)
123 adapted for ice flow (Tuckett et al., 2019; Davison et al., 2020). Computationally efficient subpixel
124 displacement estimates were made by obtaining an initial estimate of the cross-correlation peak using a
125 fast Fourier transform and then upsampling by a factor of 50 the discrete Fourier transform using matrix
126 multiplication of a small neighbourhood (1.5×1.5 pixels) around the original peak location (Guizar-
127 Sicairos et al., 2008).

128 The resulting velocity estimates were filtered in several stages. Correlations with a signal-to-noise ratio
129 (defined as the ratio of the primary cross-correlation peak to the average of the remaining cross-
130 correlation field) less than 5.8 for Sentinel-1 derived data (de Lange et al., 2007) and 11 for Landsat
131 and Sentinel-2 data were removed. Remaining spurious estimates were removed primarily using an
132 image segmentation filter with segment difference thresholds approximating realistic strain values
133 (Rosenau et al., 2015), and a kernel density filter based on the paired displacements in the range and
134 azimuth directions (Adrian & Westerweel, 2011). The filtered Sentinel-1 velocity fields were
135 transformed from radar to map coordinates using the Reference Elevation Model of Antarctica (REMA)
136 100 x 100 m Digital Elevation Model (Howat et al., 2019, 2022a) and were posted on a 150×150 m
137 grid.

138 Ice velocity data from all coincident image pairs from each mission were mosaicked, co-located and
139 stacked. The stacked data were smoothed using a 3x3 pixel moving median kernel and resampled to
140 200 m. Additional filtering of the stacked data based on temporal variations in velocity magnitude and
141 flow direction removed remaining outliers (Davison et al., 2025).

142 Time series of ice motion were created by taking the mean value from within 1000 x 1000 m regions of
143 interest (ROI), ignoring pixels in lower and upper 25th percentiles values at each epoch. Where the ROI
144 contained data gaps and had more than 33% finite values, we estimated the values of missing pixels
145 through a robust linear fit between the finite values and those from a multi-year average of the stacked
146 data – we did this in order to avoid aliasing velocity gradients within the ROI as temporal changes in
147 ice speed. The resulting time-series from within each ROI were smoothed using a second degree 24-
148 day Savitsky-Golay filter. Analysis of apparent motion over non-moving bedrock areas indicates
149 average errors of 10 to 20 m yr⁻¹. We expect these values to underestimate the true error in ice-covered
150 areas, especially where the ice surface profile has changed significantly because we assume a fixed ice
151 surface for the geocoding. Tests using a range of DEMs did not significantly affect the retrieved ice
152 speed.

153 2.2 Surface elevation change



154 We calculated surface elevation change between 2 x 2 m REMA DEM strips (Howat et al., 2022b) over
155 irregular time-periods from November 2012 to August 2024. Prior to DEM differencing, individual
156 strips were co-registered in *pDEMtools* (Chudley and Howat, 2024) to the 2 x 2 m REMA mosaic over
157 bedrock areas identified using the Scientific Committee on Antarctic Research (SCAR) Antarctic
158 Digital Database (ADD) rock outcrops mask extracted from Landsat 8 imagery (Burton-Johnson et al.,
159 2016; Gerrish, 2020).

160 **2.3 Terminus position change**

161 We manually delineated glacier termini in sufficiently clear Landsat 7, Landsat 8 and Sentinel-2 optical
162 imagery from 2000 to present using the Google Earth Engine Digitisation Tool (GEEDiT) and
163 calculated width-averaged terminus position change using the multi-centreline method in the Margin
164 change Quantification Tool (MaQiT), both of which are described in more detail by Lea et al. (2018).
165 To examine terminus position changes over longer time periods, we utilised the terminus position
166 dataset described in Cook et al. (2005). Since we are focused on the impact of surges on terminus
167 position, we did not attempt to capture any seasonal terminus position fluctuations. Given that changes
168 in terminus position during surges are typically much greater than seasonal fluctuations, we do not
169 expect this choice to affect our ability to identify surge-driven terminus position changes.

170 **2.4 Auxiliary images**

171 To support our investigation of potential surging behaviour in the 20th century we visually examined
172 the glacial geomorphological features, ice margin position and ice surface characteristics in one
173 historical aerial image and three high-resolution WorldView images of Kotick Glacier. The aerial image
174 is a 1:95,000 Vinten 70 image acquired by the British Antarctic Survey (BAS) on January 18th, 1979
175 (British Antarctic Survey, 1979), which we manually georeferenced in ArcGIS Pro using exposed
176 bedrock areas. The WorldView images are ~0.6 m resolution and were acquired on 5th February 2015,
177 11th October 2019 and 31st October 2025. The 2015 image is a single-band image from WorldView-1
178 and the other two are WorldView-2 RGB images pan-sharpened with an associated panchromatic image
179 (Imagery © 2026 Vantor). We supplemented the WorldView images with a 2 x 2 m REMA strip
180 acquired on the 9th of December 2024 (Howat et al., 2019, 2022b).

181 **2.5 The surging climatic envelope and climate reanalyses**

182 We used the global climatic envelope for surge-type glaciers (henceforth referred to as the Surging
183 Climatic Envelope, SCE) produced by Guillet et al. (2025), updated from Sevestre and Benn (2015).
184 This global dataset was produced using the January 2000 to December 2023 mean of monthly ERA5-
185 Land climate reanalysis (Muñoz-Sabater et al., 2021) of the median winter total precipitation and the



186 median summer temperature, sampled at the centroid of each Randolph Glacier Inventory polygon using
187 bi-cubic interpolation. The SCE was defined by the climate conditions covering the x % highest density
188 region of all glaciers that surged in between 1990 and 2024 (Guillet et al., 2025); here we consider
189 values of x from 20 to 99.

190 To compare climatic conditions on JRI to the SCE, we calculated median winter total precipitation and
191 median summer temperature during 10-year periods in 1-year increments from 1940 to 2025 using daily
192 ERA5 reanalysis outputs (Hersbach et al., 2020). To assess whether our study glaciers fall within the
193 optimum climatic envelope for surging during each 10-year averaging period, we interpolate each
194 climatology to the centroid of each glacier – mimicking the approach used to generate the SCE –
195 allowing us to examine changes in winter precipitation and summer temperature over each glacier with
196 respect to the global climatic envelope. To assess the validity of the ERA5 temperature changes over
197 JRI, we also examined reconstructed (RECON) monthly near-surface temperature anomalies from 1958
198 to 2022 (Bromwich and Wang, 2024; Bromwich et al., 2025) and in-situ measurements of monthly-
199 mean two metre air temperature at Esperanza Station (-63.4°N , -56.98°W ; Figure 1 inset; Turner et al.,
200 2004). RECON provides only temperature anomalies; to enable comparisons with the climatic
201 envelope, we summed the RECON anomalies with our 1950-1960 climatology from ERA5. We
202 smoothed the monthly RECON and Esperanza temperatures with a 36-month moving-mean filter for
203 comparison to the SCE.

204 To identify the spatial distribution of the SCE over time, we also identified all ERA5 pixels located
205 within the optimal climatic envelope during each 10-year averaging period from 1940 to 2024. To
206 identify glaciers that could in future fall within the SCE, we examined year 2100 projections of near-
207 surface air temperature and precipitation from the Coupled Model Intercomparison Project Phase 6
208 (CMIP6) (O'Neill et al., 2016). We incorporated 31 models forced by SSP 2-4.5 and 34 models forced
209 by SSP5-8.5 (see Supplementary Table 1 for model details and citations). For each of these model
210 outputs, we determined all locations located within the SCE in the same manner as performed for ERA5
211 during recent decades. These spatial analyses of the climatic envelope location over time allowed us to
212 examine which regions and glacier basins around Antarctica have been, are, and will be exposed to
213 surge-conducive climatic conditions.

214 **3 Results**

215 Our observations of changes in glacier terminus position, ice surface velocity and elevation in
216 combination reveal that three glaciers on JRI surged between 2000 and 2025.

217 **3.1 Whisky Glacier**

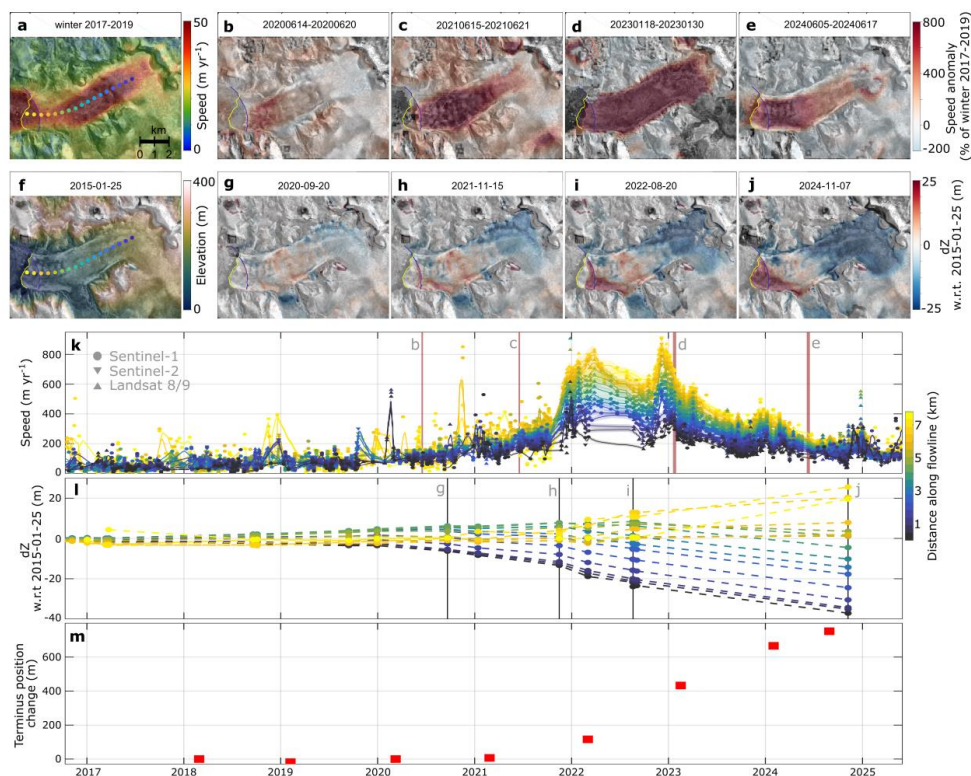


Figure 2. Whisky Glacier surge dynamics. (a) speed and (b-e) speed anomalies relative to the 2017-2019 winter mean. (f) Elevation and (g-j) elevation anomalies relative to the 2015-01-25 ice surface. The most retreated and advanced terminus positions are also shown in panels (a) and (f). (k) Speed and (l) elevation time-series along the flowline shown in (a). (m) Width-averaged terminus position change.

218 The long-term terminus position record (Cook et al., 2005), indicates sustained retreat of Whisky
 219 Glacier since 1945, within the resolution of the measurements (Supplementary Figure 1). Whisky
 220 Glacier was flowing around 40 m yr⁻¹ between 2017 and 2019 (Figure 2a), but began to accelerate in
 221 the 2019/2020 summer, reaching speeds of up to 200 m yr⁻¹ by the following autumn. During the
 222 2021/2022 summer, it rapidly accelerated to 800 m yr⁻¹ (Figure 2k). The acceleration was more
 223 pronounced and more sustained at the terminus (Figures 2b-e & k), but the entire glacier reached speeds
 224 greater than 800 % of the 2017 to 2019 average speed (Figure 2d). Clear seasonal speed changes are
 225 superimposed on the longer-term acceleration, resulting in peak speeds during the 2021/2022 and
 226 2022/2023 summers; the latter summer in particular was characterised by a sudden, large speed-up to
 227 over 900 m yr⁻¹ from November to December 2022. After the 2022/2023 summer, ice surface speeds
 228 decreased (with superimposed summer speed-ups) and along-glacier speed gradients diminished. Since
 229 approximately mid-2024, ice-surface speeds have stabilised at around four times pre-event values.
 230 During this period of dramatic speed change, the Whisky Glacier terminus advanced by more than 600
 231 m between 2021 and 2025 (Figure 2k).

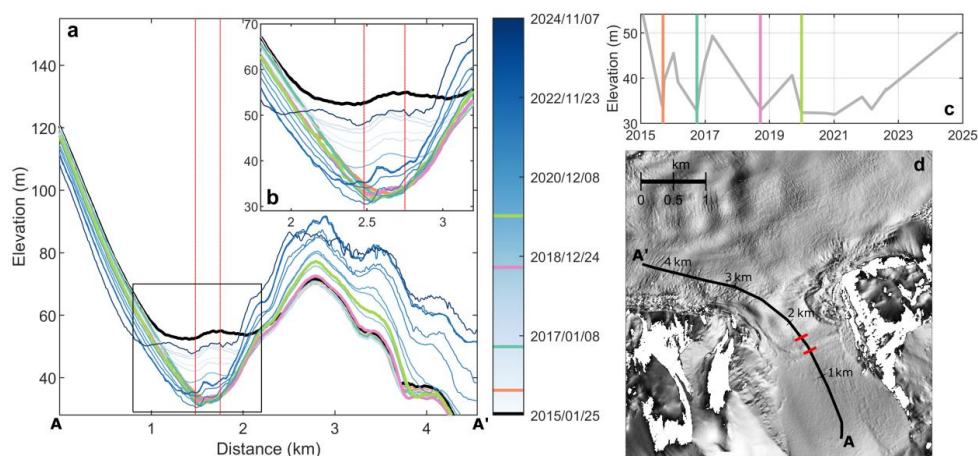


Figure 3. Surface elevation changes over a subglacial lake in Carro Pass (location in Figure 1), Whisky Glacier. (a) and (b) Show profiles of ice surface elevation along the black line in panel (d), with the elevation low stands coloured. (c) Elevation time-series extracted over the potential subglacial lake - extracted between the red lines in (d) – with the low stands marked by coloured vertical lines. (d) The flowline is overlain on a hillshade of a 2 x 2 m REMA strip (2022-09-03) (Howat et al., 2022b).

232 Concurrent with the changes in speed and terminus position of Whisky Glacier, we observed a
 233 redistribution of mass from the upper to lower parts of the glacier (Figure 2g-j & l). The uppermost
 234 reaches lowered by almost 40 m between 2020 and 2025, with the greatest rates of lowering during the
 235 2021/2022 summer through 2022. Drawdown rates diminished down-glacier and the lowest few
 236 kilometres of the glacier increased in elevation by over 20 m from 2022 onwards. Surface elevation
 237 increases were concentrated downstream of the tributary (Carro Pass) (Figure 2i,j), where there was a
 238 coincident drainage of a likely subglacial lake (Figure 3). Evidence that meltwater was stored in the
 239 subglacial lake and perhaps elsewhere beneath Whisky Glacier is provided by observations of extensive
 240 turbid meltwater plumes at the glacier terminus during the period of anomalously high flow speeds
 241 (Supplementary Figure 2).

242 3.2 Gourdon Glacier

243 The terminus position dataset of Cook et al. (2005), derived in part from georeferenced aerial imagery,
 244 shows a ~900 m advance of Gourdon Glacier from 1964 to 1974 (Supplementary Figure 1). There are
 245 no uncertainty estimates for these traces and no measurements between 1964 and 1974. The next trace
 246 (1977) indicates the terminus had by this time returned to around the 1964 position. Thus, we cannot
 247 determine whether the 1974 trace represents an advancing or retreating terminus, or if apparent advance
 248 from 1964 to 1974 occurred steadily during the ten-year period or rapidly during a short period prior to
 249 1974, or if the 1974 trace is erroneous.

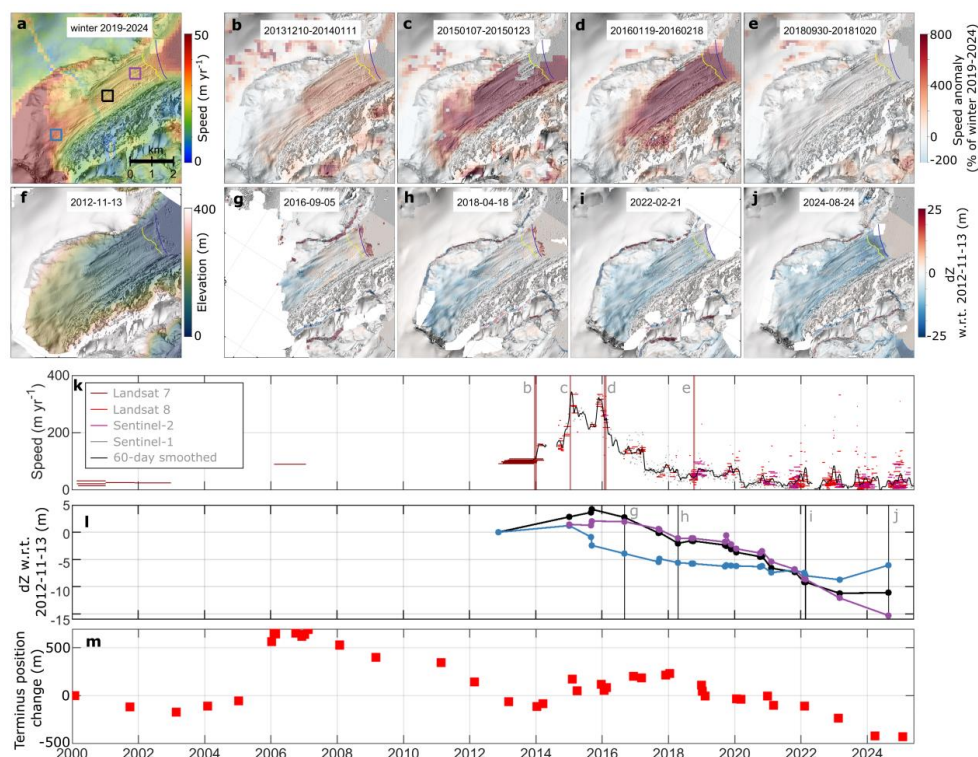


Figure 4. Gourdon Glacier surge dynamics. (a) speed and (b-e) speed anomalies relative to the 2019-2024 winter mean. (f) Elevation and (g-j) elevation anomalies relative to the 2012-11-13 ice surface. The most retreated and advanced terminus positions are also shown in panels (a) and (f). (k) Speed time-series from the black box in (a). (l) Elevation time-series from the coloured boxes shown in (a). (m) Width-averaged terminus position change.

250 Between 2000 and 2005, Gourdon Glacier was flowing at $\sim 25 \text{ yr}^{-1}$ and the terminus was relatively
 251 stationary - it retreated 170 m between 2000 and 2003 before readvancing to within 55 m of its initial
 252 position by 2005. Between January 2005 and January 2006, the terminus advanced 560 m on average
 253 and then a further 130 m by February 2007 (Figure 4m). The glacier terminus then steadily retreated
 254 until 2014, at which point its location was similar to that in 2000 (Figure 4m). The only velocity
 255 measurement during that time is from 2006 when the velocity was almost quadruple (90 m yr^{-1}) the
 256 speed measured in 2000 (Figure 4k).

257 Gourdon Glacier underwent a phase of acceleration, ice surface elevation change and terminus position
 258 change between 2013 and 2020. Ice surface speed increased between 2013 and 2016, reaching peak
 259 speeds of 325 m yr^{-1} in 2015 (13 times the average speed during 2000 to 2005), before speeds returned
 260 to $\sim 25 \text{ m yr}^{-1}$ by 2020 (Figure 4k). We note that our velocity data do not capture the beginning of this
 261 acceleration – speeds were already four times greater in 2013 than those observed in 2000. Clear
 262 summertime speed-ups in 2014/2015 and 2015/2016 were superimposed on the period of elevated



263 speeds. Interestingly, flow speed decreased in a step-wise manner, interrupted by periods of a few
264 months to over a year in which flow speed was relatively constant. From 2015 to 2017, Gourdon Glacier
265 thinned by 2.4 m in its upper reaches (blue line in Figure 4i) whilst the central and lower portions of the
266 tongue thickened by almost five metres (black and magenta lines in Figure 4i). Thinning of the entire
267 glacier occurred from 2017 to 2023, with thinning of up to ten metres in the lowest part of the glacier.
268 Since March 2023, the upper reaches of the glacier have been thickening by 2.7 m yr⁻¹ and, if those
269 rates continue, the glacier will regain its pre-surge ice thickness in September 2029 (Figure 4i,
270 Supplementary Figure 3). The terminus advanced by 180 m from March 2015 to January 2018, before
271 retreating through to 2025 (Figure 4m).

272 3.3 Kotick Glacier

273 Our measurements show a phase of synchronous speed, elevation and terminus position changes at
274 Kotick Glacier between 2014 and 2018 (Figure 5). Speed measurements for Kotick Glacier are only
275 available from 2014 onwards. In 2014, ice surface speed near the terminus was 100 to 150 m yr⁻¹, which
276 then increased to 300 m yr⁻¹ in 2015 before decelerating to 25 m yr⁻¹ between 2015 and 2018. Speed
277 remained steady at 25 m yr⁻¹ from 2018 to the end of our observation period (Figure 5k). Peak speeds
278 during 2015 diminished with distance upstream of the terminus, but remained over 200 % greater than
279 those observed since 2018 (Figure 5b-e & k). We observed terminus advance of 1000 m from 2013 to
280 2016, when a calving event disrupted the advance that continued through 2019 (Figure 5m). As with
281 Whisky Glacier, we observed surface lowering of over 20 m in the upper reaches of the glacier (Figures
282 5g-j & l). The apparent thickening in the lower reaches of the glacier shown in Figures 5g-j is due to
283 terminus advance.

284 Unlike Gourdon Glacier and Whisky Glacier, the terrain around Kotick Glacier hosts many landforms
285 from an earlier period of glaciation (Figure 1c; Figure 6). We examined these landforms and glacier
286 geometry in aerial and satellite imagery to investigate glacier geometry and behaviour prior to our
287 observations of ice surface elevation and velocity. A WorldView image acquired on 5th February 2015
288 shows a series of short (~70 m), narrow (< 25 m) linear ridges oriented at a range of angles obliquely
289 to ice flow to the true-left of Kotick Glacier (Figure 6). These ridges are approximately symmetrical in
290 cross-section with an amplitude of 2 m (Figure 6d). The ridges were visible prior to the 2013 to 2017
291 advance of Kotick Glacier, though two of the ridges were partially overridden during that advance. A
292 georeferenced aerial image acquired in January 1979 (Supplementary Figure 4) provides indirect
293 evidence that the area hosting these ridges was overridden at the time: the image does not directly
294 capture the area hosting the ridges, but it clearly shows Kotick Glacier approximately 350 m from the
295 present-day ridges (Supplementary Figure 4). Based on the geometry of the visible part of Kotick
296 Glacier in 1979 and the elevation difference (40 m) between the edge of the imaged glacier and the

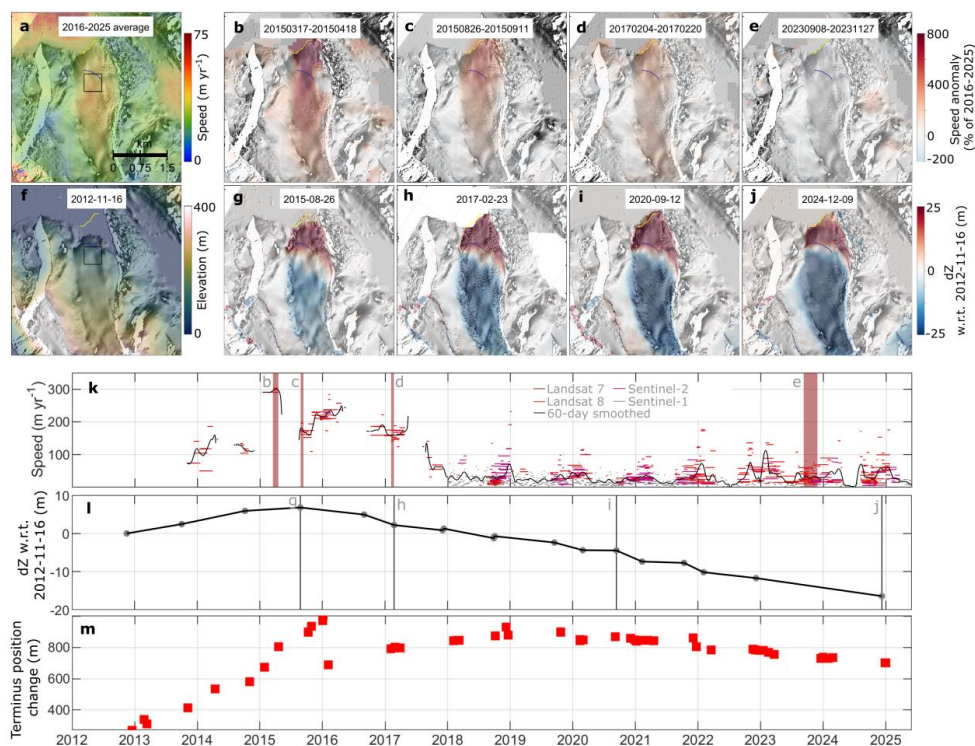


Figure 5. Kotick Glacier surge dynamics. (a) speed and (b-e) speed anomalies relative to the 2016-2025 trimmed mean speed (excluding the lower and upper 25th percentiles). (f) Elevation and (g-j) elevation anomalies relative to the 2012-11-16 ice surface. The most retreated and advanced terminus positions are also shown in panels (a) and (f). (k) Speed and (l) elevation time-series from the black box shown in (a). (m) Width-averaged terminus position change.

297 ridges, it is plausible that Kotick Glacier occupied the location of the ridges in January 1979. Based on
 298 these observations, it seems likely that the ridges formed between 1979 and 2000, when our terminus
 299 position observations show the area hosting the ridges was not ice covered.

300 4 Discussion

301 4.1 Glacier surge characteristics

302 Our observations of change in glacier terminus position, ice surface velocity and elevation in
 303 combination reveal that three glaciers on JRI surged between 2005 and 2025. The surge phase of these
 304 glaciers lasted approximately four years, with a progressive acceleration to peak speeds that persisted
 305 for approximately one year or two summers, followed by a comparatively prolonged deceleration in
 306 which speeds remained substantially greater than pre-surge values for more than three years. These
 307 characteristics of the surge phase are typical of tidewater glacier surges and differ from typical land-
 308 terminating surge phases, which generally have shorter deceleration phases lasting less than two years

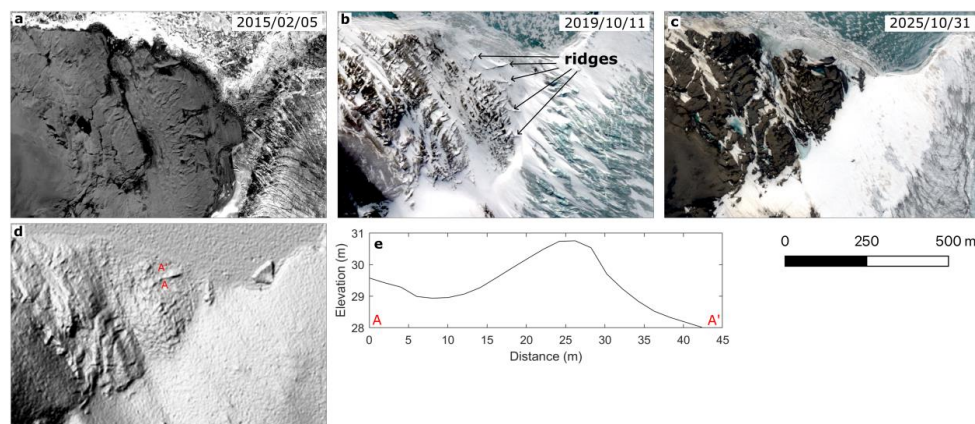


Figure 6. Candidate crevasse-squeeze ridges (CSRs) adjacent to Kotick Glacier (location in Figure 1c). Panel (a) shows a WorldView-1 image and panels (b) and (c) show WorldView-2 images with candidate CSRs labelled. Panel (d) shows a hillshade (three times vertical exaggeration) of a Reference Elevation Model of Antarctica strip (2024-12-09) with the location of the elevation transect shown in panel (e). Imagery © 2026 Vantor.

309 (Guillet et al., 2025). In comparison to specific, well-known glacier surges: the duration of the surge
 310 phases observed here are longer than those observed on the land-terminating Variegated Glacier, Alaska
 311 (1-2 years) (Kamb et al., 1985; Eisen et al., 2001), but comparable to those of the marine-terminating
 312 Monacobreen and Morsnevbreen, Svalbard (Benn et al., 2019b, 2022). Our observational record is
 313 generally too short to robustly determine the duration of the quiescent phase of these glaciers; our data
 314 suggest that Gourdon Glacier surged twice since 2005 with a seven-year quiescent phase, implying that
 315 another surge may be imminent. However, the upper reaches of the glacier did not begin to regain mass
 316 until 2023, and the observed thickening rate (2.7 m yr^{-1}) implies that pre-surge thicknesses will not be
 317 reached again until September 2029 (Figure 4i, Supplementary Figure 3).

318 Our observations suggest that the surge of Whisky Glacier was initiated at or a short distance upstream
 319 of the terminus. During the rising limb of the surge, the acceleration of Whisky Glacier was clearly
 320 greater in the lower reaches of the glacier than in the upper reaches (Figure 2). We also observed
 321 frequent and increasingly extensive turbid plumes at the Whisky Glacier terminus from 2020 through
 322 2023 (during the surge) as well as a large calving event near the plume in December 2021
 323 (Supplementary Figure 2). These observations highlight the role of basal enthalpy, supplemented by
 324 efficient surface-to-bed meltwater connections associated with more extensive crevassing and enhanced
 325 generation of basal meltwater through rapid ice motion (Dunse et al., 2015; Sevestre et al., 2018).

326 We note that a likely subglacial lake in Carro Pass drained between September 14th 2019 and December
 327 30th 2019 (Figure 3), which coincides approximately with the onset of the Whisky Glacier surge (ice
 328 velocity tripled during 2020). This may have contributed to the greater acceleration of the lower reaches
 329 of Whisky Glacier; however, given that this lake drained approximately annually during our



330 observational period, and because the late-2019 drainage was smaller than in previous years (Figure 3),
331 it seems unlikely that the lake drainage was the primary cause of the surge. There are, however, clear
332 indications that the surge affected the subglacial hydrological connections between the subglacial lake
333 and Whisky Glacier. Ice surface elevation over the lake did not begin to recover until the 2021/2022
334 summer, indicating that the evacuation of stored basal meltwater during the surge seemed to prevent
335 lake refilling throughout 2020. Ice surface elevations over the lake have since returned to pre-surge
336 levels, indicating complete or partial refill of the lake (Figure 3).

337 **4.2 Spatial extent of surging on the Antarctic Peninsula and neighbouring islands**

338 To our knowledge, only the surge of Kotick Glacier has previously been described as an unambiguous
339 surge (Stringer et al., 2025). The higher resolution velocity data used here allows us to substantially
340 revise the estimated tripling in speed to a 12-fold increase (Figure 5). Stringer et al. (2025) also reported
341 the recent advance of Whisky Glacier but lacked the auxiliary data to confirm surging behaviour. Earlier
342 work (Nichols, 1973) proposed that Northeast Glacier, flowing into Marguerite Bay, may be a surge-
343 type glacier based on observations (Nichols, 1960) of coherent iceberg and sea ice motion adjacent to
344 the advancing glacier terminus. Our velocity data do not reveal any surging behaviour at Northeast
345 Glacier (not shown) and the ice delta described by Nichols (1960) appears to reform in most years, so
346 may reflect sea ice conditions and retention of icebergs near the seasonally-advancing terminus, rather
347 than a sudden increase in calving activity associated with a surge.

348 We conducted a preliminary exploration for other glacier surges on the Antarctic Peninsula by exploring
349 ice speed time-series to identify candidate surges. Of the hundreds of glaciers examined, we found only
350 two glaciers (Supplementary Figure 5) with speed time-series characterised by very slow motion
351 followed by a substantial increase in velocity lasting more than 1 year. These may constitute surging
352 behaviour, but we have not examined terminus position or elevation change measurements, which
353 would allow us to rule out other processes, such as temporary ungrounding or retreat. Both of the
354 glaciers that exhibit surge-like ice velocity variations are located on islands surrounding the northern
355 tip of the Antarctic Peninsula (Supplementary Figure 5). We did not find evidence of surging elsewhere
356 on the Antarctica Peninsula, but acknowledge that the sparsity of velocity data prior to 2016 could result
357 in missed surges and future studies could incorporate a larger range of observations to produce a
358 comprehensive inventory of Antarctic glacier surges.

359 **4.3 Onset and frequency of surging on James Ross Island in relation to 20th century climate change**

360 Given that glacier surges are a recently identified phenomenon in Antarctica, we discuss the potential
361 influence of climate change on their occurrence. This discussion is motivated in part by several
362 published examples of apparent changes in surge frequency that were temporally associated with



363 changes in climate or mass balance. The most striking of these examples is the cessation of surging at
364 Vernagtferner in the Ötztal Alps, which surged from the 17th to the 19th century but has not surged since;
365 this senescence was attributed to both rising atmospheric temperatures and glacier mass loss (Hoinkes,
366 1969). More recent works have examined changes in surge frequency over comparatively shorter
367 periods that were not always significantly longer than the quiescent phase. Putting aside the potential
368 observation bias inherent in those (and any) attempts, they indicate a cessation of surging activity of
369 small glaciers in Svalbard due to thinning since the Little Ice Age (Dowdeswell et al., 1995; James et
370 al., 2012; Benn et al., 2019a) and increasing surge frequency in the late-20th century in the Karakoram,
371 associated with a period of anomalously high modelled precipitation (Copland et al., 2011). Several
372 other examples are discussed in a comprehensive review (Lovell et al., 2026). When viewed under the
373 lens of statistical analyses showing that surge-type glaciers occupy a distinct (though broad) climatic
374 envelope (Sevestre and Benn, 2015; Guillet et al., 2025) and the theoretical basis by which those
375 conditions encourage the build-up of a mass and enthalpy imbalance that culminates in a surge (Benn
376 et al., 2019a; 2022), these examples of apparent changes in surge frequency globally begin to build up
377 a picture of how the surging behaviour of glaciers on JRI might have changed in response to changing
378 climatic conditions over the last century.

379 To evaluate how climatic changes over the last century might have affected the surging behaviour of
380 JRI glaciers, we compared ERA5 reanalysis of two-metre air temperature and precipitation over JRI in
381 10-year averaging periods to the globally defined SCE (Guillet et al., 2025; Figure 7a). This analysis
382 indicates that these glaciers have been exposed to conditions at the cooler end of the SCE since at least
383 the beginning of the reanalysis period (1940) and have pushed further into the SCE as atmospheric
384 temperatures have risen and precipitation has increased (Figure 7a). Comparisons with air temperature
385 measurements at Esperanza Station (100 km from JRI; location in Figure 1) and an Antarctic-specific
386 near-surface air temperature reconstruction (RECON; Bromwich et al., 2025) confirm the approximate
387 magnitude and timing of the air temperature trend shown in ERA5 (Figure 7a). Thus, as predicted by
388 Sevestre and Benn (2015), glacier surging on JRI at any time since 1940 is consistent with the enthalpy
389 balance theory of glacier surging (Benn et al., 2019a; 2022), because the climate appears to have been
390 conducive to the development of a mass and basal enthalpy imbalance since the beginning of the
391 reanalysis period. Further progression of these glaciers into the SCE (i.e. towards warmer, more humid
392 conditions; Figure 7a) implies a greater rate of basal enthalpy accumulation and increased surge activity.
393 Enthalpy balance theory predicts that basal hydrological processes may hinder a smooth transition to
394 higher velocities, forcing the glaciers to undergo velocity fluctuations to discharge mass over longer
395 cycles.

396 There is therefore a theoretical basis on which to expect an increase in the prevalence of surging on JRI
397 over the last century. As with previous work, this study suffers from observation bias due to the increase

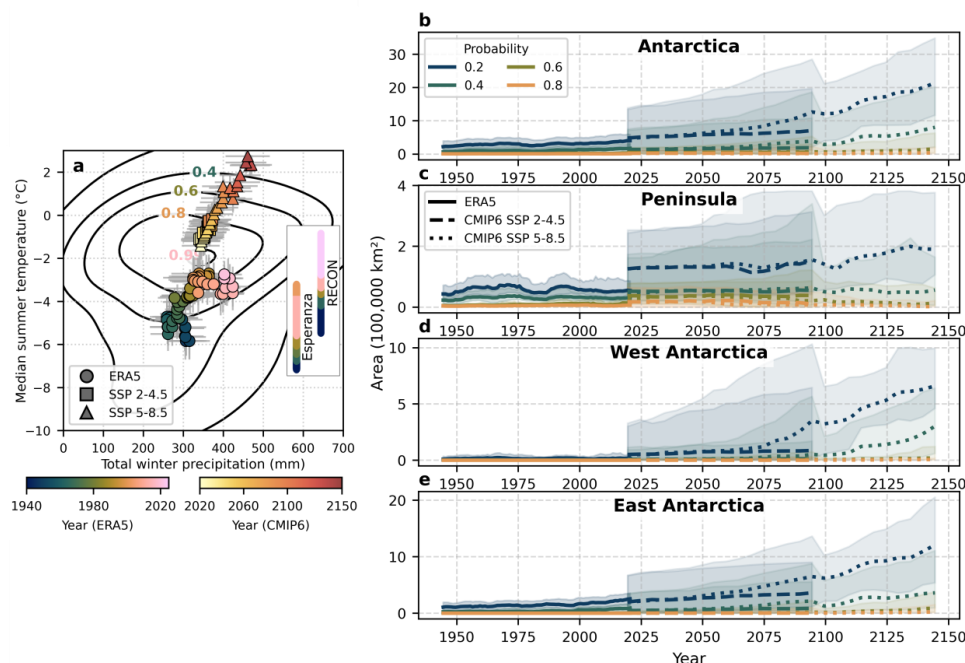


Figure 7. (a) The trajectory of the climate of James Ross Island (JRI) with respect to the optimal envelope for glacier surging (SCE). The black contours show the boundaries of the SCE at each probability level (coloured as in panel (b)). The coloured dots show the climate of JRI in ten-year periods from 1940 to 2025, in one-year increments, from ERA5. The coloured squares and triangles show the ensemble mean climate of JRI in ten-year periods from 2020 to 2100 (SSP2-4.5) and 2150 (SSP5-8.5) from a suite of CMIP6 simulations (detailed in Supplementary Table 1). The inset panel shows the temperature change over time recorded at Esperanza Station and reconstructed (RECON), both smoothed with a 36-month moving mean filter. Note the RECON data include only temperature anomalies from 1956 onwards – we have added them to the ERA5 data here to illustrate the potential range of temperatures on JRI over time. The time-series show the area of grounded ice exposed to the SCE in (b) Antarctica, (c) the Antarctic Peninsula, (d) West Antarctica and (e) East Antarctica.

398 in observations over time, which limits our ability to evaluate changes in surge frequency over the last
 399 century. Two of our observations (glacial landforms at Kotick Glacier and terminus advance of Gourdon
 400 Glacier) suggest that surging may have occurred on JRI in the second half of the 20th century. The first
 401 piece of evidence for 20th century surging on JRI comes from the glacial geomorphological record
 402 adjacent to Kotick Glacier. We observed a group of five short (~70 m), low amplitude (2 m) ridges on
 403 the true-left of Kotick Glacier (Figure 6). These ridges are oriented obliquely to the present-day ice flow
 404 direction. Two of the ridges were partially overridden during the 2013 to 2017 surge of Kotick Glacier
 405 (Figure 6). Based on these characteristics, we suggest they are crevasse-squeeze ridges (CSRs) (Rea
 406 and Evans, 2011; Evans et al., 2016; Rivers et al., 2023), which are thought to be the infills of basal
 407 crevasses preserved at the termination of a surge (e.g. Benediktsson et al., 2009). A single BAS aerial
 408 image acquired in January 1979 shows the upper reaches of the glacier in a geometry that strongly
 409 indicates the area hosting the CSRs was covered by Kotick Glacier in January 1979 (Supplementary
 410 Figure 4). Given the poor preservation potential of CSRs in terrestrial environments, we argue that the



411 candidate CSRs therefore likely formed in a surge during or after 1979, but prior to the 2013 to 2017
412 surge. The surface of Kotick Glacier in the 1979 aerial image does not appear to be heavily crevassed
413 in its upper reaches, which would be expected during and immediately following a surge. If a surge did
414 occur between 1979 and 2000, it was not apparent from the 1988 terminus position trace of Cook et al.
415 (2005). We note that if surging of JRI tidewater glaciers occurred in the past, then the landform record
416 would predominantly be submarine. To our knowledge there is no suitably high-resolution bathymetric
417 data adjacent to these glaciers with which to interrogate the submarine landform record but future
418 studies could acquire this information to help to clarify the surge history of JRI glaciers.

419 The second piece of evidence for 20th century surging on JRI is provided by observations of the terminus
420 position of Gourdon Glacier (Cook et al., 2005; Supplementary Figure 1). The terminus of Gourdon
421 Glacier advanced by 900 m from 1964 to 1974, which could be indicative of a surge. We treat this
422 inference with caution, however, because we do not have corresponding ice surface elevation or velocity
423 measurements to confirm this advance was caused by a surge. The long duration between these terminus
424 position observations and the lack of terminus position uncertainty estimates further limit our ability to
425 attribute this apparent advance to a surge of Gourdon Glacier. This advance could, amongst other
426 factors, have been caused instead by interannual variations in sea ice extent or simply errors in the
427 georectification of the oblique aerial imagery used to delineate the glacier terminus.

428 Overall, it is clear that four surges at three glaciers on JRI have occurred since 2005 (Figures 2, 4 & 5)
429 and there is some, albeit inconclusive, evidence that two of these glaciers may have surged in the second
430 half of the 20th century. The glaciers on JRI have been exposed to the SCE since at least the 1940s but
431 have progressed further into the SCE over time (Figure 7a). From a theoretical and statistical
432 perspective, surging was therefore possible in the 20th century and the probability of surging has
433 increased as the climate has become warmer and wetter (Benn et al., 2019a, 2022; Guillet et al., 2025).
434 Our observations are consistent with the hypothesis that changes in climate over the past century have
435 increased the likelihood or frequency of surging on JRI. However, we have few constraints on the timing
436 and frequency of surging during the 20th century and a more detailed reconstruction of 20th century
437 Antarctic Peninsula surging, derived from archive aerial imagery and field observations of the
438 submarine and subaerial landform record, would be required to confirm a change in surge frequency
439 over the last century, which would provide an informative test case for theories seeking to explain
440 surging behaviour.

441 **4.4 Changes to the locations exposed to the surging climatic envelope through the 20th and 21st** 442 **centuries**

443 Although the location of the SCE is not a definitive predictor of surging behaviour, we examine how
444 climate change through the 20th century and projected climate changes over the 21st century have



445 affected and will affect the locations exposed to climatic conditions conducive to glacier surging
446 (Figures 8 & 9; Supplementary Videos). We preface this discussion by noting that the SCE is defined
447 at surge-type glacier centroids, which approximate the equilibrium line altitude (e.g. Carrivick and
448 Brewer, 2004), whereas surging is a whole-glacier phenomenon. Thus, the SCE provides the climate
449 over a small subset of the area occupied by surge-type glaciers. As consequence, spatial maps of the
450 SCE, such as those discussed here, will tend to underestimate the potential extent of surging and a given
451 glacier may be susceptible to surging if the SCE encroaches into the ablation zone and towards the
452 equilibrium line altitude, even if the entire basin is not encompassed by the SCE. The SCE was also
453 defined for a population of predominantly valley glaciers up to a few tens of kilometres in length
454 (Guillet et al., 2025). Glacier size exerts a strong secondary influence on the propensity for a glacier to
455 surge (Benn et al., 2019a); therefore, we must be cautious when attempting to extrapolate the SCE to
456 Antarctic glaciers, particularly those outside of the Peninsula, many of which are much larger than the
457 glaciers used to define the SCE.

458 With these caveats in mind, the restriction of observed surging behaviour to the warmest, northernmost
459 parts of Antarctica and surrounding islands is broadly consistent with the present-day and historical
460 spatial distribution of ERA5 temperature and precipitation with respect to the SCE (Figure 7a; Figure
461 8). ERA5 shows a steady southward migration of the areas exposed to the SCE from 1940 to 2020
462 (Figure 8) and a corresponding increase ($92 \text{ km}^2 \text{ yr}^{-1}$, $p < 0.05$; Supplementary Table 2) in the area of
463 grounded ice on the Peninsula exposed to the SCE (Figure 7c; Supplementary Videos 1-5). In the 1940s,
464 the SCE began to encroach on JRI at the 0.6 SCE probability level, though climate variability in the
465 1940s intermittently exposed JRI to conditions closer to the centre of the SCE (Figure 7a) and lower
466 probability SCE levels encompass JRI throughout the reanalysis period (Figure 8). The SCE contracted
467 southwards through the last quarter of the 20th century, encompassing JRI and the northernmost tip of
468 the Peninsula, while extending along the eastern coastline as far south as Larsen-C Ice Shelf but with
469 minimal transgression onto grounded ice (Figure 8d; Supplementary Videos 1-5). Elsewhere around
470 Antarctica, the SCE remained seaward of the coast until 2020 at the 0.6 SCE probability level (Figures
471 8a & b; Supplementary Video 8). Low-to-moderate probability SCE transgression onto the Larsen,
472 Wilkins and George VI ice shelves, and the ice shelves of Dronning Maud Land, Victoria Land and
473 parts of Wilkes Land occurred in the late-20th or early-21st century (Figure 8; Supplementary Videos 6-
474 8). As the SCE contracted southwards, the South Shetland Islands and South Orkney Islands have
475 become exposed to conditions further from the centre of the SCE (Figure 8c). For comparison, similar
476 shifts in climate across Greenland have been associated with a change in spatial extent of surge
477 envelopes and with the number of surge-type glaciers per sub-region (Lovell et al., 2023).

478 Analyses of CMIP6 model output allows us to briefly explore the potential for changes in surge
479 occurrence around Antarctica throughout the 21st century under modest (SSP2-4.5) and extreme (SSP5-

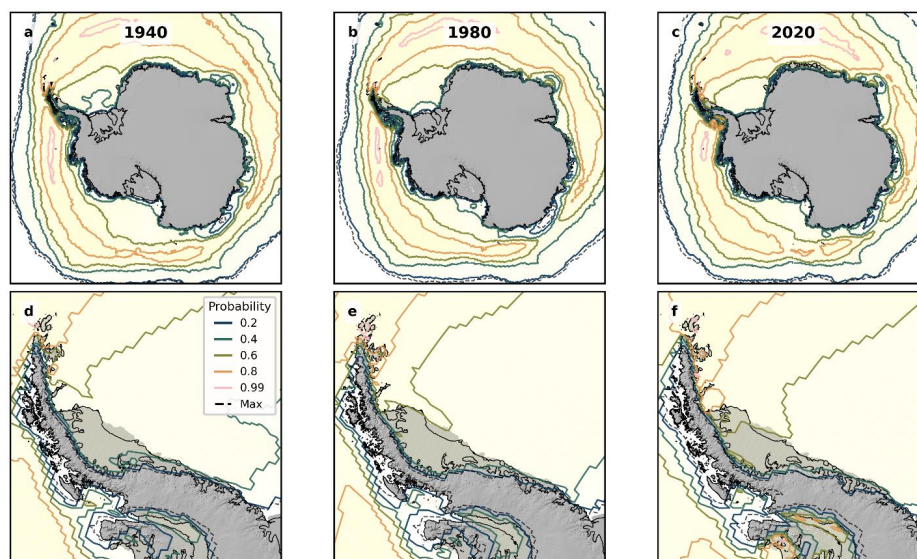


Figure 8. Mapping the optimal surging climatic envelope (SCE) around Antarctica with ERA5. Each panel shows the location of SCE for the labelled decade. The solid-coloured contours show the edge of the SCE for each probability level. The dashed contours show the maximum extent of the 0.2 probability SCE when the standard deviation of temperature and precipitation within the decade is considered alongside the decadal mean climate.

480 8.5) warming scenarios (Figure 9; Supplementary Videos 11-30). We note there is a positive
 481 temperature bias of 1.6°C and 1.3°C in the CMIP6 SSP2-4.5 and SSP5-8.5 ensemble means compared
 482 to ERA5 (Supplementary Figure 6), that hinders comparisons or the computation of long-term trends
 483 (Figure 7). ERA5 is known to underestimate mid-20th century temperature and overestimate late-20th
 484 century temperature around Antarctica (Bromwich et al., 2024); however, the mismatch with
 485 temperature recorded at stations is smallest on the Peninsula (Bromwich et al., 2024). At three stations
 486 with long-term temperature records (Esperanza, Faraday/Vernadsky and Orcadas), ERA5 has a mean
 487 bias of -0.19 ± 1.42 °C at Faraday, -0.18 ± 1.60 °C at Orcadas and -1.02 ± 1.33 °C at Esperanza and the
 488 temperature trends are within 0.006 °C decade⁻¹ at Orcadas and Esperanza and almost within error at
 489 Faraday (Supplementary Figure 7; Supplementary Table 3). Thus, the offset between ERA5 and the
 490 CMIP6 ensemble mean is likely predominantly due to overestimation of temperature in CMIP6. This
 491 could be due to the coarser resolution of the CMIP6 simulations, which will resolve the effects of steep
 492 topography less effectively than ERA5.

493 Keeping in mind the temperature offset between ERA5 and CMIP6, the CMIP6 output shows a
 494 continuation of the spatiotemporal trends in SCE exposure exhibited by ERA5 throughout the 20th
 495 century (Figure 7-9; Supplementary Video 1). Over JRI, the combination of ERA5 and CMIP6 output
 496 show a climate trajectory pushing deeper into, through then further from the SCE core from 1940
 497 through 2150 (Figure 7). When variability amongst CMIP6 ensemble members is considered, there is

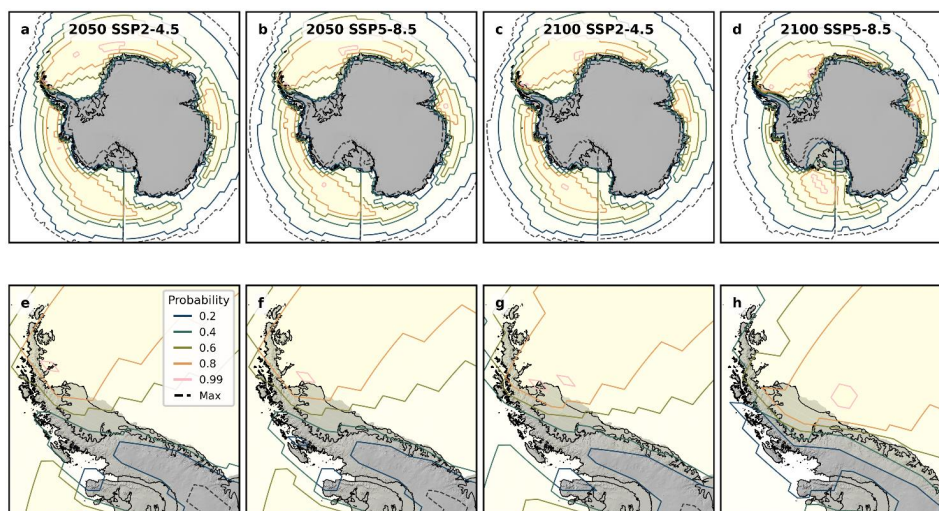


Figure 9. Mapping the optimal surging climatic envelope (SCE) around Antarctica with CMIP6 output. Each panel shows the location of SCE for the labelled decade and SSP scenario. The solid-coloured contours show the edge of the SCE for each probability level. The dashed contours show the maximum extent of the 0.2 probability SCE when the standard deviation of the ensemble mean temperature and precipitation is considered alongside the ensemble mean climate.

498 little divergence between emissions scenarios in projections of the SCE extent up to the middle of the
 499 21st century. In both emission scenarios, both east and west coasts of the Antarctic Peninsula as far
 500 south as the Larsen-B Embayment enter the SCE at the 0.6 probability level before 2050 (Figure 9;
 501 Supplementary Videos 13 & 23). Many more glaciers further south on the Peninsula and ice streams in
 502 Dronning Maud Land and West Antarctica have complete or partial exposure to the SCE at lower
 503 probability levels (Supplementary Videos 16, 17, 26 & 27), but we reiterate our reservations about
 504 extrapolating the relationship between climate and surging to large ice streams. Rising air temperatures
 505 through the first half of the 21st century cause the South Shetland Islands and South Orkney Islands to
 506 approach the edge of the SCE in both emission scenarios (Figures 9a & b). Beyond 2050, changes to
 507 the areas of Antarctica exposed to the SCE are relatively minor in SSP2-4.5 (Figures 7b & 9c). Under
 508 extreme warming (SSP5-8.5), JRI and much the Peninsula warm sufficiently to lower their exposure to
 509 the SCE, whilst the southward contraction of the SCE exposes progressively more of the East Antarctic
 510 and West Antarctic coastlines to climate conditions conducive to glacier surging (Figures 9d & h;
 511 Supplementary Video 1), dramatically increasing the area of grounded ice exposed to the SCE (Figures
 512 7b-e).

513 The historical and projected changes to the locations of Antarctica exposed to the SCE provide a crude
 514 indication of how surge occurrence and frequency have and may continue to change around Antarctica
 515 in response to climate change. The historical changes to climate through the 20th and early-21st century,
 516 resulting in greater exposure of JRI and surrounding islands to the SCE and increased likelihood of



517 surging (Figures 7 & 8), is broadly consistent with the timing and location of glacier surges observed
518 here. Analysis of CMIP6 model output with respect to the SCE suggests that we might expect an
519 increase in the number of surge-type glaciers on the Antarctic Peninsula throughout the remainder of
520 the 21st century in moderate warming scenarios (Figure 9). If atmospheric warming continues unabated,
521 the climate of the Antarctic Peninsula is likely to become less conducive to surging beyond 2050, which
522 may result in a reduction in surge frequency and extent. The ice shelves and coastline of East Antarctica
523 and West Antarctica will become increasingly exposed to the SCE especially in SSP5-8.5; however, it
524 is unlikely that the SCE defined for valley glaciers can be applied to much larger ice streams.

525 **5 Conclusion**

526 We present observations of surging between 2005 and 2025 at Whisky Glacier, Gourdon Glacier and
527 Kotick Glacier on James Ross Island, Antarctica. The surges exhibit all the characteristics typical of
528 tidewater glacier surges, particularly a rapid acceleration over the course of a year, peak speeds lasting
529 up to two summers, redistribution of mass from higher to lower elevations along with terminus advance,
530 and a prolonged deceleration phase lasting several years. Gourdon Glacier has likely surged twice since
531 2005 with a ten-year quiescent phase. There is reasonable, yet inconclusive, evidence that Kotick
532 Glacier and perhaps Gourdon Glacier surged between the 1970s and 2000s. The occurrence and timing
533 of the surges observed and inferred here are consistent with the enthalpy balance theory for glacier
534 surges because these glaciers have occupied and pushed deeper into the optimal climatic envelope for
535 glacier surging since at least the 1940s. Based on examination of the historical and projected spatial
536 distribution of atmospheric conditions associated with surging, we hypothesise that surging will become
537 more prevalent on the Antarctic Peninsula over the coming decades. Under extreme warming, however,
538 surge occurrence on the Antarctic Peninsula may decline in the second half of the 21st century. We
539 suggest that continued monitoring of Antarctic Peninsula ice surface elevation and speed change will
540 enable detection, and perhaps prediction, of surging in the coming decades. Finally, surge behaviour
541 should not be ignored when interpreting observations of glacier geometry change and the landform
542 record in future studies of northern Antarctic Peninsula glacier dynamics.

543

544 **Code Availability**

545 The code required to reproduce the analyses presented in this paper will be archived in a Zenodo
546 repository upon publication. The open-source GMTSAR code is available from
547 <https://topex.ucsd.edu/gmtsar/>. PIVsuite, which provided the basis for our feature tracking software, is
548 available from <https://uk.mathworks.com/matlabcentral/fileexchange/45028-pivsute>. pDEMtools is
549 documented in <https://pdemtools.readthedocs.io/en/v1.2.3/>.

550



551 **Data availability**

552 The data required to reproduce the analyses presented in this paper will be archived in a Zenodo
 553 repository upon publication. Sentinel-1 images are freely available from
 554 <https://dataspace.copernicus.eu/data-collections/copernicus-sentinel-missions/sentinel-1> and
 555 <https://asf.alaska.edu/>. Sentinel-2 images are freely available from [https://dataspace.copernicus.eu/data-](https://dataspace.copernicus.eu/data-collections/copernicus-sentinel-missions/sentinel-2)
 556 [collections/copernicus-sentinel-missions/sentinel-2](https://dataspace.copernicus.eu/data-collections/copernicus-sentinel-missions/sentinel-2) and <https://browser.dataspace.copernicus.eu/>.
 557 Landsat 7 and 8 images are freely available from <https://earthexplorer.usgs.gov/>. REMA DEM strips
 558 and mosaics are freely available from <https://www.pgc.umn.edu/data/rema/>. Historical aerial images
 559 acquired by BAS are freely available from <https://earthexplorer.usgs.gov/>. ERA5 monthly gridded
 560 temperature and precipitation fields are freely available from
 561 <https://cds.climate.copernicus.eu/datasets/reanalysis-era5-single-levels-monthly-means?tab=overview>.
 562 CMIP6 model output is freely available from [https://cds.climate.copernicus.eu/datasets/projections-](https://cds.climate.copernicus.eu/datasets/projections-cmip6?tab=overview)
 563 [cmip6?tab=overview](https://cds.climate.copernicus.eu/datasets/projections-cmip6?tab=overview). Temperature observations from Esperanza Station, Orcadas and
 564 Faraday/Vernadsky are freely available from <http://www.nerc-bas.ac.uk/icd/gjma/>. RECON data are
 565 freely available from [https://amrddata.ssec.wisc.edu/dataset/reconstruction-of-antarctic-near-surface-](https://amrddata.ssec.wisc.edu/dataset/reconstruction-of-antarctic-near-surface-air-temperatures-at-monthly-intervals-since-1958)
 566 [air-temperatures-at-monthly-intervals-since-1958](https://amrddata.ssec.wisc.edu/dataset/reconstruction-of-antarctic-near-surface-air-temperatures-at-monthly-intervals-since-1958).

567

568 **Author contribution**

569 The contributions of all authors are described in the CRediT table below.

CRediT matrix	Benjamin J. Davison	Andrew J. Sole	Gregoire Guillet	Douglas I. Benn	Jonathan Kingslake	Jeremy Ely	Stephen J. Livingstone	Christopher D. Stringer	Jonathan Carrivick	Anna E. Hogg
Conceptualization	1	1		1		1		1	1	1
Data curation	1		1							
Formal analysis	1									
Funding acquisition		1			1	1	1			
Investigation	1							1		
Interpretation	1	1	1	1	1	1	1	1	1	1
Methodology	1	1								
Project administration		1			1					
Resources										
Software	1	1								
Supervision										
Validation	1									
Visualization	1									
Writing (pre-submission)	1	1	1	1	1	1	1	1	1	1
Writing (revisions)										



570

571

572

573 **Competing interests**

574 At least one author is a member of the editorial board of The Cryosphere.

575 **Acknowledgements**

576 We acknowledge IT Services at The University of Sheffield for the provision of services for High
577 Performance Computing. Geospatial support for this work was provided by the Polar Geospatial Center
578 under NSF-OPP award 2053169. The authors gratefully acknowledge the European Space Agency and
579 the European Commission for the acquisition, generation, and availability of Copernicus Sentinel-1 and
580 Sentinel-2 data.

581

582 **Financial support**

583 This work was funded by NSFGEO-NERC Grant Number #2053169, "Investigating the Direct
584 Influence of Meltwater on Antarctic Ice Sheet Dynamics".

585

586 **References**

587 Benediktsson, Í.Ö., Ingólfsson, O., Schomacker, A. and Kjaer, K.H., 2009. Formation of submarginal
588 and proglacial end moraines: implications of ice-flow mechanism during the 1963–64 surge of
589 Brúarjökull, Iceland. *Boreas*, 38(3), pp.440-457.

590 Benn, D.I., Hewitt, I.J. and Luckman, A.J., 2022. Enthalpy balance theory unifies diverse glacier surge
591 behaviour. *Annals of Glaciology*, 63(87-89), pp.88-94.

592 Benn, D.I., Fowler, A.C., Hewitt, I. and Sevestre, H., 2019a. A general theory of glacier surges. *Journal*
593 *of Glaciology*, 65(253), pp.701-716.

594 Benn, D.I., Jones, R.L., Luckman, A., Fürst, J.J., Hewitt, I. and Sommer, C., 2019b. Mass and enthalpy
595 budget evolution during the surge of a polythermal glacier: a test of theory. *Journal of Glaciology*,
596 65(253), pp.717-731.

597 Boxall, K., Christie, F.D., Willis, I.C., Wuite, J. and Nagler, T., 2022. Seasonal land-ice-flow variability
598 in the Antarctic Peninsula. *The Cryosphere*, 16(10), pp.3907-3932. DOI: <https://doi.org/10.5194/tc-16-3907-2022>.

600 Boxall, K., Christie, F.D., Willis, I.C., Wuite, J., Nagler, T. and Scheiblauer, S., 2024. Drivers of
601 seasonal land-ice-flow variability in the Antarctic Peninsula. *Journal of Geophysical Research:*
602 *Earth Surface*, 129(6), p.e2023JF007378. DOI: <https://doi.org/10.1029/2023JF007378>.



- 603 Braun, M., Humbert, A. and Moll, A., 2009. Changes of Wilkins Ice Shelf over the past 15 years and
604 inferences on its stability. *The Cryosphere*, 3(1), pp.41-56. DOI: [https://doi.org/10.5194/tc-3-41-](https://doi.org/10.5194/tc-3-41-2009)
605 [2009](https://doi.org/10.5194/tc-3-41-2009).
- 606 British Antarctic Survey, 1979. BAS/JR/1/79 January 1979. 1:95000 Vertical air photograph of James
607 Ross Island item 18. British Antarctic Survey. Cambridge.
- 608 Bromwich, D.H., Ensign, A., Wang, S.H. and Zou, X., 2024. Major artifacts in ERA5 2-m air
609 temperature trends over Antarctica prior to and during the modern satellite era. *Geophysical*
610 *Research Letters*, 51(21), p.e2024GL111907. DOI: <https://doi.org/10.1029/2024GL111907>.
- 611 Bromwich, David and Wang, Sheng-Hung, 2024: Reconstruction of Antarctic Near-Surface Air
612 Temperatures at Monthly Intervals Since 1958. *AMRDC Data Repository*, accessed 02-03-2026,
613 <https://doi.org/10.48567/efwt-jw56>.
- 614 Bromwich, D., Wang, S.H., Zou, X. and Ensign, A., 2025. An updated reconstruction of Antarctic near-
615 surface air temperatures at monthly intervals since 1958. *Earth System Science Data*, 17(6),
616 pp.2953-2962. DOI: <https://doi.org/10.5194/essd-17-2953-2025,%202025>.
- 617 Burton-Johnson, A., Black, M., Fretwell, P.T. and Kaluza-Gilbert, J., 2016. An automated methodology
618 for differentiating rock from snow, clouds and sea in Antarctica from Landsat 8 imagery: a new rock
619 outcrop map and area estimation for the entire Antarctic continent. *The Cryosphere*, 10(4), pp.1665-
620 1677.
- 621 Carrivick, J.L. and Brewer, T.R., 2004. Improving local estimations and regional trends of glacier
622 equilibrium line altitudes. *Geografiska Annaler: Series A, Physical Geography*, 86(1), pp.67-79.
- 623 Carrivick, J.L., Davies, B.J., Glasser, N.F., Nývlt, D. and Hambrey, M.J., 2012. Late-Holocene changes
624 in character and behaviour of land-terminating glaciers on James Ross Island, Antarctica. *Journal of*
625 *Glaciology*, 58(212), pp.1176-1190. DOI: <https://doi.org/10.3189/2012JoG11J148>.
- 626 Chudley, T. R., and Howat, I. M. (2024). pDEMtools: conveniently search, download, and process
627 ArcticDEM and REMA products. *Journal of Open Source Software*, 9(102), 7149,
628 doi.org/10.21105/joss.07149
- 629 Cook, A.J. and Vaughan, D.G., 2010. Overview of areal changes of the ice shelves on the Antarctic
630 Peninsula over the past 50 years. *The cryosphere*, 4(1), pp.77-98. DOI: [https://doi.org/10.5194/tc-4-](https://doi.org/10.5194/tc-4-77-2010)
631 [77-2010](https://doi.org/10.5194/tc-4-77-2010).
- 632 Cook, A.J., Fox, A.J., Vaughan, D.G. and Ferrigno, J.G., 2005. Retreating glacier fronts on the Antarctic
633 Peninsula over the past half-century. *Science*, 308(5721), pp.541-544.
- 634 Cook, A.J., Vaughan, D.G., Luckman, A.J. and Murray, T., 2014. A new Antarctic Peninsula glacier
635 basin inventory and observed area changes since the 1940s. *Antarctic Science*, 26(6), pp.614-624.
636 DOI: <https://doi.org/10.1017/S0954102014000200>.
- 637 Cook, A.J., Holland, P.R., Meredith, M.P., Murray, T., Luckman, A. and Vaughan, D.G., 2016. Ocean
638 forcing of glacier retreat in the western Antarctic Peninsula. *Science*, 353(6296), pp.283-286. DOI:
639 <https://doi.org/10.1126/science.aac0017>.
- 640 Cooper, A.P.R., 1997. Historical observations of Prince Gustav ice shelf. *Polar Record*, 33(187),
641 pp.285-294. DOI: <https://doi.org/10.1017/S0032247400025389>



- 642 Copland, L., Sylvestre, T., Bishop, M.P., Shroder, J.F., Seong, Y.B., Owen, L.A., Bush, A. and Kamp,
643 U., 2011. Expanded and recently increased glacier surging in the Karakoram. *Arctic, Antarctic, and*
644 *Alpine Research*, 43(4), pp.503-516.
- 645 Davison, B.J., Hogg, A.E., Moffat, C., Meredith, M.P. and Wallis, B.J., 2024. Widespread increase in
646 discharge from west Antarctic Peninsula glaciers since 2018. *The Cryosphere*, 18(7), pp.3237-3251.
647 DOI: <https://doi.org/10.5194/tc-18-3237-2024>.
- 648 Davison, B.J., Sole, A.J., Cowton, T.R., Lea, J.M., Slater, D.A., Fahrner, D. and Nienow, P.W., 2020.
649 Subglacial drainage evolution modulates seasonal ice flow variability of three tidewater glaciers in
650 southwest Greenland. *Journal of Geophysical Research: Earth Surface*, 125(9), p.e2019JF005492.
651 DOI: <https://doi.org/10.1029/2019JF005492>.
- 652 Davison, B.J., Hogg, A.E., Gourmelen, N., Jakob, L., Wuite, J., Nagler, T., Greene, C.A., Andreasen,
653 J. and Engdahl, M.E., 2023. Annual mass budget of Antarctic ice shelves from 1997 to 2021. *Science*
654 *Advances*, 9(41), p.eadi0186. DOI: <https://doi.org/10.1126/sciadv.adi0186>.
- 655 Davison, B.J., Hogg, A.E., Slater, T., Rigby, R. and Hansen, N., 2025. Antarctic Ice Sheet grounding
656 line discharge from 1996–2024. *Earth System Science Data*, 17(7), pp.3259-3281. DOI:
657 <https://doi.org/10.5194/essd-17-3259-2025>.
- 658 de Lange, R., Luckman, A., & Murray, T. (2007). Improvement of satellite radar feature tracking for
659 ice velocity derivation by spatial frequency filtering. *IEEE Transactions on Geoscience and Remote*
660 *Sensing*, 45(7), 2309–2318. <https://doi.org/10.1109/TGRS.2007.896615>
- 661 Doake, C.S.M. and Vaughan, D.G., 1991. Breakup of Wordie Ice Shelf, Antarctica. *IAHS Publ*, 208,
662 pp.161-165.
- 663 Dowdeswell, J.A., Hodgkins, R., Nuttall, A.M., Hagen, J.O. and Hamilton, G.S., 1995. Mass balance
664 change as a control on the frequency and occurrence of glacier surges in Svalbard, Norwegian High
665 Arctic. *Geophysical Research Letters*, 22(21), pp.2909-2912.
- 666 Dunse, T., Schellenberger, T., Hagen, J.O., Kääh, A., Schuler, T.V. and Reijmer, C.H., 2015. Glacier-
667 surge mechanisms promoted by a hydro-thermodynamic feedback to summer melt. *The Cryosphere*,
668 9(1), pp.197-215.
- 669 Eisen, O., Harrison, W.D. and Raymond, C.F., 2001. The surges of Variegated Glacier, Alaska, USA,
670 and their connection to climate and mass balance. *Journal of Glaciology*, 47(158), pp.351-358.
- 671 Evans, D.J., Storrar, R.D. and Rea, B.R., 2016. Crevasse-squeeze ridge corridors: diagnostic features
672 of late-stage palaeo-ice stream activity. *Geomorphology*, 258, pp.40-50. DOI:
673 <https://doi.org/10.1016/j.geomorph.2016.01.017>.
- 674 Fowler, A.C., Murray, T. and Ng, F.S.L., 2001. Thermally controlled glacier surging. *Journal of*
675 *Glaciology*, 47(159), pp.527-538. DOI: <https://doi.org/10.3189/172756501781831792>.
- 676 Gardner, A. S., M. A. Fahnestock, and T. A. Scambos, 2025: MEaSURES ITS LIVE Landsat Image-
677 Pair Glacier and Ice Sheet Surface Velocities: Version 1. Data archived at National Snow and Ice
678 Data Center. <https://doi.org/10.5067/IMR9D3PEI28U>
- 679 Gerrish, L. (2020). Automatically extracted rock outcrop dataset for Antarctica (Version 7.2) [Data set].
680 UK Polar Data Centre, Natural Environment Research Council, UK Research & Innovation.
681 <https://doi.org/10.5285/9DF510E3-EA1C-450B-9950-D742DB1EFD96>.



- 682 Gerrish, L., Ireland, L., Fretwell, P., & Cooper, P. (2024). High resolution vector polylines of the
683 Antarctic coastline - VERSION 7.9 (Version 7.9) [Data set]. NERC EDS UK Polar Data Centre.
684 <https://doi.org/10.5285/45c3cc90-098b-45e3-a809-16b80eed4ec2>.
- 685 Gorodetskaya, I.V., Durán-Alarcón, C., González-Herrero, S., Clem, K.R., Zou, X., Rowe, P.,
686 Rodríguez Imazio, P., Campos, D., Leroy-Dos Santos, C., Dutrievoz, N. and Wille, J.D., 2023.
687 Record-high Antarctic Peninsula temperatures and surface melt in February 2022: a compound event
688 with an intense atmospheric river. *npj climate and atmospheric science*, 6(1), p.202. DOI:
689 <https://doi.org/10.1038/s41612-023-00529-6>.
- 690 Guillet, G., Benn, D.I., King, O., Shean, D., Mannerfelt, E.S. and Hugonnet, R., 2025. Global detection
691 of glacier surges from surface velocities, elevation change and SAR backscatter data between 2000
692 and 2024: a test of surge mechanism theories. *Journal of Glaciology*, 71, p.e88. DOI:
693 <https://doi.org/10.1017/jog.2025.10065>.
- 694 Guizar-Sicairos, M., Thurman, S. T., & Fienup, J. R. (2008). Efficient subpixel image registration
695 algorithms. *Optics Letters*, 33(2), 156. <https://doi.org/10.1364/OL.33.000156>.
- 696 Hersbach, H., Bell, B., Berrisford, P., Hirahara, S., Horányi, A., Muñoz-Sabater, J., Nicolas, J., Peubey,
697 C., Radu, R., Schepers, D., Simmons, A., Soci, C., Abdalla, S., Abellan, X., Balsamo, G., Bechtold,
698 P., Biavati, G., Bidlot, J., Bonavita, M., De Chiara, G., Dahlgren, P., Dee, D., Diamantakis, M.,
699 Dragani, R., Flemming, J., Forbes, R., Fuentes, M., Geer, A., Haimberger, L., Healy, S., Hogan, R.
700 J., Hólm, E., Janisková, M., Keeley, S., Laloyaux, P., Lopez, P., Lupu, C., Radnoti, G., de Rosnay,
701 P., Rozum, I., Vamborg, F., Villaume, S., and Thépaut, J. N.: The ERA5 global reanalysis, *Q. J. R.*
702 *Meteorol. Soc.*, 146, 1999–2049, <https://doi.org/10.1002/qj.3803>, 2020.
- 703 Hogg, A.E., Shepherd, A., Cornford, S.L., Briggs, K.H., Gourmelen, N., Graham, J.A., Joughin, I.,
704 Mouginot, J., Nagler, T., Payne, A.J. and Rignot, E., 2017. Increased ice flow in Western Palmer
705 Land linked to ocean melting. *Geophysical Research Letters*, 44(9), pp.4159-4167. DOI:
706 <https://doi.org/10.1002/2016GL072110>.
- 707 Hoinkes, H. C. 1969. Surges of the Vernagtferner in the Otztal Alps since 1599. *Can. J. Earth Sci.*, 6(4,
708 Part 2), pp.853–861.
- 709 Howat, I.M., Porter, C., Smith, B.E., Noh, M.J. and Morin, P., 2019. The reference elevation model of
710 Antarctica. *The Cryosphere*, 13(2), pp.665-674. DOI: <https://doi.org/10.5194/tc-13-665-2019>.
- 711 Howat, Ian, et al., 2022a, “The Reference Elevation Model of Antarctica – Mosaics, Version 2”,
712 <https://doi.org/10.7910/DVN/EBW8UC>, Harvard Dataverse, V1, 16/03/2022.
- 713 Howat, Ian, et al., 2022b, “The Reference Elevation Model of Antarctica – Strips, Version 4.1”,
714 <https://doi.org/10.7910/DVN/X7NDNY>, Harvard Dataverse, V1, 16/03/2022.
- 715 James, T.D., Murray, T., Barrand, N.E., Sykes, H.J., Fox, A.J. and King, M.A., 2012. Observations of
716 enhanced thinning in the upper reaches of Svalbard glaciers. *The Cryosphere*, 6(6), pp.1369-1381.
717 DOI: <https://doi.org/10.5194/tc-6-1369-2012>.
- 718 Jiskoot, H. 2011. 'Glacier Surging', in Bishop, M.P., Björnsson, H., Haeberli, W., Oerlemans, J.,
719 Shroder, J.F. and Tranter, M. *Encyclopedia of snow, ice and glaciers*. Springer Science & Business,
720 pp. 415-428.
- 721 Kamb, B., Raymond, C.F., Harrison, W.D., Engelhardt, H., Echelmeyer, K.A., Humphrey, N.,
722 Brugman, M.M. and Pfeffer, T., 1985. Glacier surge mechanism: 1982-1983 surge of Variegated
723 Glacier, Alaska. *Science*, 227(4686), pp.469-479.



- 724 Kuipers Munneke, P., Luckman, A.J., Bevan, S.L., Smeets, C.J.P.P., Gilbert, E., Van Den Broeke, M.R.,
725 Wang, W., Zender, C., Hubbard, B., Ashmore, D. and Orr, A., 2018. Intense winter surface melt on
726 an Antarctic ice shelf. *Geophysical Research Letters*, 45(15), pp.7615-7623. DOI:
727 <https://doi.org/10.1029/2018GL077899>.
- 728 Lea, J.M., 2018. The Google Earth Engine Digitisation Tool (GEEDiT) and the Margin change
729 Quantification Tool (MaQiT)—simple tools for the rapid mapping and quantification of changing
730 Earth surface margins. *Earth Surface Dynamics*, 6(3), pp.551-561.
- 731 Lovell, H., Carrivick, J.L., King, O., Sutherland, J.L., Yde, J.C., Boston, C.M. and Malecki, J., 2023.
732 Surge-type glaciers in Kalaallit Nunaat (Greenland): distribution, temporal patterns and climatic
733 controls. *Journal of Glaciology*, 69(278), pp.1785-1802.
- 734 Lovell, H., Benn, D.I., Jiskoot, H., Stokes, C.R., Flowers, G.E., Guillet, G., Mannerfelt, E.S., Falaschi,
735 D., Kääh, A., King, O. and Benediktsson, Í.Ö., 2026. Glacier surging and surge-related hazards in a
736 changing climate. *Nature Reviews Earth & Environment*, pp.1-19. DOI:
737 <https://doi.org/10.1038/s43017-025-00757-9>.
- 738 MacAyeal, D.R., Scambos, T.A., Hulbe, C.L. and Fahnestock, M.A., 2003. Catastrophic ice-shelf
739 break-up by an ice-shelf-fragment-capsize mechanism. *Journal of Glaciology*, 49(164), pp.22-36.
740 DOI: <https://doi.org/10.3189/172756503781830863>.
- 741 Mougintot, J., Scheuchl, B. & Rignot, E. 2017. MEaSURES Antarctic Boundaries for IPY 2007-2009
742 from Satellite Radar. (NSIDC-0709, Version 2). [Data Set]. Boulder, Colorado USA. NASA
743 National Snow and Ice Data Center Distributed Active Archive Center.
744 <https://doi.org/10.5067/AXE4121732AD>. Date Accessed 03-18-2026.
- 745 Muñoz-Sabater, J., Dutra, E., Agustí-Panareda, A., Albergel, C., Arduini, G., Balsamo, G., Boussetta,
746 S., Choulga, M., Harrigan, S., Hersbach, H. and Martens, B., 2021. ERA5-Land: A state-of-the-art
747 global reanalysis dataset for land applications. *Earth system science data*, 13(9), pp.4349-4383.
- 748 Murray, T., Strozzi, T., Luckman, A., Jiskoot, H. and Christakos, P., 2003. Is there a single surge
749 mechanism? Contrasts in dynamics between glacier surges in Svalbard and other regions. *Journal*
750 *of Geophysical Research: Solid Earth*, 108(B5). DOI: <https://doi.org/10.1029/2002JB001906>.
- 751 Nichols, R.L., 1960. Geomorphology of Marguerite Bay area, Palmer Peninsula, Antarctica. *Geological*
752 *Society of America Bulletin*, 71(10), pp.1421-1450.
- 753 Nichols, R.L., 1973. Antarctic glacial surges?. *Journal of Glaciology*, 12(66), pp.524-525.
754 doi:10.3189/S0022143000031981.
- 755 Ochwat, N.E., Scambos, T.A., Banwell, A.F., Anderson, R.S., MacLennan, M.L., Picard, G., Shates,
756 J.A., Marinsek, S., Margonari, L., Truffer, M. and Pettit, E.C., 2023. Triggers of the 2022 Larsen B
757 multi-year landfast sea ice break-out and initial glacier response. *The cryosphere discussions*, 2023,
758 pp.1-34. DOI: <https://doi.org/10.5194/tc-18-1709-2024>.
- 759 O'Neill, B.C., Tebaldi, C., Van Vuuren, D.P., Eyring, V., Friedlingstein, P., Hurtt, G., Knutti, R.,
760 Kriegler, E., Lamarque, J.F., Lowe, J. and Meehl, G.A., 2016. The scenario model intercomparison
761 project (ScenarioMIP) for CMIP6. *Geoscientific Model Development*, 9(9), pp.3461-3482. DOI:
762 <https://doi.org/10.5194/gmd-9-3461-2016>.
- 763 Rack, W. and Rott, H., 2004. Pattern of retreat and disintegration of the Larsen B ice shelf, Antarctic
764 Peninsula. *Annals of glaciology*, 39, pp.505-510. DOI:
765 <https://doi.org/10.3189/172756404781814005>.



- 766 Rea, B.R. and Evans, D.J., 2011. An assessment of surge-induced crevassing and the formation of
767 crevasse squeeze ridges. *Journal of Geophysical Research: Earth Surface*, 116(F4).
- 768 Rignot, E., Casassa, G., Gogineni, P., Krabill, W., Rivera, A.U. and Thomas, R., 2004. Accelerated ice
769 discharge from the Antarctic Peninsula following the collapse of Larsen B ice shelf. *Geophysical
770 research letters*, 31(18). DOI: <https://doi.org/10.1029/2004GL020697>.
- 771 Rivers, G.E., Storrar, R.D., Jones, A.H. and Ojala, A.E., 2023. 3D morphometry of De Geer Moraines
772 and Crevasse-Squeeze Ridges: Differentiating between pushing and squeezing mechanisms from
773 remotely sensed data. *Quaternary Science Reviews*, 321, p.108383.
- 774 Rosenau, R., Scheinert, M., & Dietrich, R. (2015). A processing system to monitor Greenland outlet
775 glacier velocity variations at decadal and seasonal time scales utilizing the Landsat imagery. *Remote
776 Sensing of Environment*, 169, 1–19. <https://doi.org/10.1016/j.rse.2015.07.012>.
- 777 Rott, H., Skvarca, P. and Nagler, T., 1996. Rapid collapse of northern Larsen ice shelf,
778 Antarctica. *Science*, 271(5250), pp.788-792. DOI: <https://doi.org/10.1126/science.271.5250.788>.
- 779 Rott, H., Abdel Jaber, W., Wuite, J., Scheiblaue, S., Floricioiu, D., Van Wessem, J.M., Nagler, T.,
780 Miranda, N. and Van Den Broeke, M.R., 2018. Changing pattern of ice flow and mass balance for
781 glaciers discharging into the Larsen A and B embayments, Antarctic Peninsula, 2011 to 2016. *The
782 Cryosphere*, 12(4), pp.1273-1291. DOI: <https://doi.org/10.5194/tc-12-1273-2018>.
- 783 Rott, H., Wuite, J., De Rydt, J., Gudmundsson, G.H., Floricioiu, D. and Rack, W., 2020. Impact of
784 marine processes on flow dynamics of northern Antarctic Peninsula outlet glaciers. *Nature
785 communications*, 11(1), p.2969. DOI: <https://doi.org/10.1038/s41467-020-16658-y>.
- 786 Sandwell, D., Mellors, R., Tong, X., Wei, M. and Wessel, P., 2011a. GMTSAR: An InSAR processing
787 system based on generic mapping tools. Retrieved from <https://escholarship.org/uc/item/8zq2c02m>.
- 788 Sandwell, D., Mellors, R., Tong, X., Wei, M., & Wessel, P. 2011b. Open radar interferometry software
789 for mapping surface deformation. *Eos, Transactions American Geophysical Union*, 92(28), 234.
790 <https://doi.org/10.1029/2011EO280002>
- 791 Scambos, T.A., Bohlander, J.A., Shuman, C.A. and Skvarca, P., 2004. Glacier acceleration and thinning
792 after ice shelf collapse in the Larsen B embayment, Antarctica. *Geophysical Research
793 Letters*, 31(18). DOI: <https://doi.org/10.1029/2004GL020670>.
- 794 Seehaus, T., Cook, A.J., Silva, A.B. and Braun, M., 2018. Changes in glacier dynamics in the northern
795 Antarctic Peninsula since 1985. *The Cryosphere*, 12(2), pp.577-594. DOI:
796 <https://doi.org/10.5194/tc-12-577-2018>.
- 797 Sevestre, H. and Benn, D.I., 2015. Climatic and geometric controls on the global distribution of surge-
798 type glaciers: implications for a unifying model of surging. *Journal of Glaciology*, 61(228), pp.646-
799 662. DOI: <https://doi.org/10.3189/2015JoG14J136>.
- 800 Sevestre, H., Benn, D. I., Luckman, A., Nuth, C., Kohler, J., Lindbäck, K., & Pettersson, R. 2018.
801 Tidewater glacier surges initiated at the terminus. *Journal of Geophysical Research: Earth Surface*,
802 123, 1035–1051. <https://doi.org/10.1029/2017JF004358>.
- 803 Stringer, C.D., Macfee, M.W., Carrivick, J.L., Láska, K., Engel, Z., Matějka, M., Harpur, C., Nývlt, D.,
804 Quincey, D.J. and Davies, B.J., 2025. Accelerated glacier changes on the James Ross Archipelago,
805 Antarctica, from 2010 to 2023. *Journal of Glaciology*, 71, p.e102.



- 806 Sun, Y., Riel, B. and Minchew, B., 2023. Disintegration and buttressing effect of the landfast sea ice in
807 the Larsen B embayment, Antarctic Peninsula. *Geophysical Research Letters*, 50(16),
808 p.e2023GL104066. DOI: <https://doi.org/10.1029/2023GL104066>.
- 809 Surawy-Stepney, T., Hogg, A.E., Cornford, S.L., Wallis, B.J., Davison, B.J., Selley, H.L., Slater, R.A.,
810 Lie, E.K., Jakob, L., Ridout, A. and Gourmelen, N., 2024. The effect of landfast sea ice buttressing
811 on ice dynamic speedup in the Larsen B embayment, Antarctica. *The Cryosphere*, 18(3), pp.977-
812 993. DOI: <https://doi.org/10.5194/tc-18-977-2024>.
- 813 Thielicke, W., & Stamhuis, E. J. (2014). PIVlab—Towards user-friendly, affordable and accurate
814 digital particle image velocimetry in MATLAB. *Journal of Open Research Software*, 2(1), e30.
815 <https://doi.org/10.5334/jors.bl>.
- 816 Tuckett, P.A., Ely, J.C., Sole, A.J., Livingstone, S.J., Davison, B.J., Melchior van Wessem, J. and
817 Howard, J., 2019. Rapid accelerations of Antarctic Peninsula outlet glaciers driven by surface
818 melt. *Nature Communications*, 10(1), p.4311. DOI: <https://doi.org/10.1038/s41467-019-12039-2>.
- 819 Tuckett, P.A., Ely, J.C., Sole, A.J., Livingstone, S.J., Davison, B.J., & Melchior van Wessem, J. 2020.
820 Reply to: “Impact of marine processes on flow dynamics of northern Antarctic Peninsula outlet
821 glaciers” by Rott et al.. *Nature Communications* 11, 2970 (2020). [https://doi.org/10.1038/s41467-](https://doi.org/10.1038/s41467-020-16685-9)
822 [020-16685-9](https://doi.org/10.1038/s41467-020-16685-9);
- 823 Turner, J., Colwell, S.R., Marshall, G.J., Lachlan-Cope, T.A., Carleton, A.M., Jones, P.D., Lagun, V.,
824 Reid, P.A. and Iagovkina, S., 2004. The SCAR READER project: toward a high-quality database of
825 mean Antarctic meteorological observations. *Journal of Climate*, 17(14), pp.2890-2898. DOI:
826 [https://doi.org/10.1175/1520-0442\(2004\)017%3C2890:TSRPTA%3E2.0.CO;2](https://doi.org/10.1175/1520-0442(2004)017%3C2890:TSRPTA%3E2.0.CO;2).
- 827 Wallis, B.J., Hogg, A.E., van Wessem, J.M., Davison, B.J. and van den Broeke, M.R., 2023a.
828 Widespread seasonal speed-up of west Antarctic Peninsula glaciers from 2014 to 2021. *Nature*
829 *Geoscience*, 16(3), pp.231-237. DOI: <https://doi.org/10.1038/s41561-023-01131-4>.
- 830 Wallis, B.J., Hogg, A.E., Meredith, M.P., Close, R., Hardy, D., McMillan, M., Wuite, J., Nagler, T. and
831 Moffat, C., 2023. Ocean warming drives rapid dynamic activation of marine-terminating glacier on
832 the west Antarctic Peninsula. *Nature Communications*, 14(1), p.7535. DOI:
833 <https://doi.org/10.1038/s41467-023-42970-4>.
- 834 Adrian, R. J., & Westerweel, J. (2011). Particle image velocimetry. *Cambridge: Cambridge University*
835 *Press*.
- 836 Wuite, J., Rott, H., Hetzenecker, M., Floricioiu, D., De Rydt, J., Gudmundsson, G.H., Nagler, T. and
837 Kern, M., 2015. Evolution of surface velocities and ice discharge of Larsen B outlet glaciers from
838 1995 to 2013. *The Cryosphere*, 9(3), pp.957-969. DOI: <https://doi.org/10.5194/tc-9-957-2015>.
- 839
- 840